GEOCHEMISTRY

On the role of α-alumina in the origin of life: Surface-driven assembly of amino acids

Ruiyu Wang[1,2], Richard C. Remsing[3], Michael L. Klein[1,2,4], Eric Borguet[1,2]*, Vincenzo Carnevale[4,5]*

We investigate the hypothesis that mineral/water interfaces played a crucial catalytic role in peptide formation by promoting the self-assembly of amino acids. Using classical molecular dynamics simulations, we demonstrate that the α-alumina(0001) surface exhibits an affinity of 4 k_BT for individual glycine or GG dipeptide molecules due to hydrogen bonds. In simulations with multiple glycine molecules, surface-bound glycine enhances further adsorption, leading to the formation of long chains connected by hydrogen bonds between the carboxyl and amine groups of glycine molecules. We find that the likelihood of observing chains longer than 10 glycine units increases by at least five orders of magnitude at the surface compared to the bulk. This surface-driven assembly is primarily due to local high density and alignment with the alumina surface pattern. Together, these results propose a model for how mineral surfaces can induce configuration-specific assembly of amino acids, thereby promoting condensation reactions.

INTRODUCTION

The question of how life emerged on planet Earth has intrigued scientists for decades (*1*–*4*). In this regard, understanding the spontaneous formation of the macromolecules that underpin life's crucial biochemical processes will inform the better design of bioinspired materials (*5*–*7*) as well as aid in the search for habitable exoplanets (*8*, *9*). To fold into thermodynamically stable structures and thus to have well-defined biochemical properties, peptides should be at least 40 amino acids long (*10*).

The Miller-Urey experiments showed that only monomeric amino acids form when models of early Earth atmospheres (H_2O, CH_4, NH_3, and H_2) are heated and exposed to an electric discharge (*11*–*14*). Later, Saitta and colleagues provided crucial microscopic insight into these processes by confirming that large electrostatic fields can notably lower the barrier to generate formamide, CO, and NH_3 using molecular dynamics (MD) simulations (*12*, *15*). However, polypeptides were not observed in these experiments, and the possible origins of polypeptide formation on the early Earth remain a mystery.

Polypeptide chains are formed by amino acid monomers through condensation reactions (Fig. 1). For a linear polymer chain, the chain length distribution can be estimated using the Flory model (*16*, *17*)

$$N_n / N = (1-p)p^{n-1} \quad (1)$$

where n is the number of monomeric units in a chain, N_n is the number of polymers with n units, N is the total number of polymer and monomer molecules, and p is the probability for condensation reactions. Equation 1 shows that the probability of finding a chain with a certain length decreases exponentially with the chain length. Forming a chain longer than 40 amino acids would be an exceedingly rare event, unlikely to occur even on geological timescales. A partial solution to this conundrum is the autocatalysis mechanism, that is, polymer chains with more than 10 units promote the adsorption of monomer using the chain itself as the template, thereby making chains longer than 30 more likely to occur (*10*).

The issue that remains unclear is how polypeptides can reach the critical length of 10 units. The condensation reaction (Fig. 1) is both thermodynamically unfavorable and kinetically slow, primarily due to a free energy barrier of approximately 50 kcal/mol, which inhibits spontaneous reactions in bulk water (*18*). Increasing the temperature not only accelerates the reaction but also facilitates the drying of the surface and the removal of by-product water, thereby also making the reaction thermodynamically favorable (*19*). One hypothesis is that the origin of polypeptide comes from mineral surfaces near hydrothermal vent in the deep sea (*8*, *20*). High temperature and solid surfaces can accelerate amino acid condensation reactions (*13*, *21*–*28*). For instance, heating glycine solutions in the presence of oxide mineral powders resulted in the formation of peptides and by-product diketopiperazine (DKP), a glycine dimer that does not lead to polypeptide chains. The activity of multiple earth-abundant oxides was examined, and the activity follows the sequence $TiO_2 > Al_2O_3 > SiO_2$ (*29*). While TiO_2 shows the highest overall catalytic activity, it is notably less abundant than Al_2O_3 in the Earth's crust. Moreover, Al_2O_3 shows very little production of the by-product DKP. From this, we believe that Al_2O_3 is a promising candidate as a natural amino acid condensation catalyst.

Previous observations show that ions prefer to nucleate at solid surfaces (*30*) or aggregate to form specific patterns under confinement without any templates (*31*). Our hypothesis is that besides lowering the reaction barrier by altering reaction pathways (*32*), solid surfaces can promote the noncovalent self-assembly of monomers (*33*–*37*). Such adsorption and pre-assembly of amino acids at

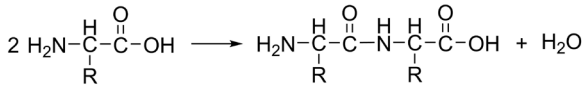

Fig. 1. The amino acid condensation reaction. Two glycine molecules generate a GG dipeptide.

[1]Department of Chemistry, Temple University, Philadelphia, PA 19122, USA. [2]Center for Complex Materials from First Principles (CCM), Temple University, Philadelphia, PA 19122, USA. [3]Department of Chemistry and Chemical Biology, Rutgers University, Piscataway, NJ 08854, USA. [4]Institute for Computational Molecular Science, Temple University, Philadelphia, PA 19122, USA. [5]Department of Biology, Temple University, Philadelphia, PA 19122, USA.
*Corresponding author. Email: eborguet@temple.edu (E.B.); vincenzo.carnevale@temple.edu (V.C.)

alumina surfaces align monomers to orientations that are favorable for polymerization.

Here, we address two key questions regarding Al_2O_3-catalyzed amino acid condensation reactions: (i) Do amino acids prefer to remain in solution or adsorb onto the alumina surface? (ii) Does the alumina surface promote the aggregation of ordered structures of adsorbed amino acids? To investigate these questions, we focused on the α-alumina(0001) surface, which is the most stable phase of alumina. Its flat (0001) surface has been extensively studied and provides an ideal model for our simulations (*38*). The (0001) surface strongly promotes adsorption of sodium halides on the hexagonal pattern of aluminol groups (*39*), and interfaces facilitate the nucleation of solid NaCl, making the aggregation state dominated at reduced dimensional environments (*31*, *40*). We carried out MD simulations with metadynamics, an enhanced sampling technique that enables sampling of diverse molecular configurations while preserving their statistical weights (*41*–*43*). We find that glycine, the simplest amino acid, shows an affinity for the alumina surface of 4 k_BT due to the hydrogen bonds (H-bonds) established with the surface. Adsorbed glycine molecules further promote adsorption, thereby increasing local concentration. In addition to glycine-surface H-bonds, glycine molecules form H-bonds with one another. Pairings between carboxyl and amine groups give rise to aggregates with diverse morphologies, such as chains and clusters. Compared to bulk solutions, the probability of finding a chain of 10 glycine units is enhanced by at least 10^5 times due to the increased concentration resulting from adsorption.

We also find a positive correlation between the formation of long chain and an ordered pattern of glycine adsorption. Finally, simulations show that glycine molecules that belong to long chains have a lower number of solvation-shell waters, indicating that hydration hinders the formation of chains.

RESULTS

Adsorption of a single glycine molecule

We calculated the free energy surface (FES) of the zwitterionic forms of a single glycine (GLY) and GLY-GLY (GG) dipeptide (Fig. 2) The zwitterionic form is selected because it is stable at pH 7. Two collective variables (CVs), Z and θ_{NC}, are applied to describe the binding configurations of the glycine. They represent the distance between surface oxygen and the center of mass of the glycine, and the molecule's out-of-plane orientation, defined as the angle between the surface normal and the **NC** vector, where N and C atoms are from the terminal amine and carboxyl groups (Fig. 2B). The one-dimensional (1D) FES shows that the free energy is lower at the surface than in the bulk for both glycine and GG dipeptide with a free energy difference of 4 k_BT (Fig. 2A), indicating a strong affinity between amino acids and the alumina surface. At $Z = 0.32$ nm, the global minimum of the 1D FES and the closest to the surface, the glycine is oriented parallel to the solid surface, simultaneously donating and accepting H-bonds to and from the surface through the amino (N terminus) and carboxyl group (C terminus) (fig. S5). Similar configurations have been observed in density functional theory (DFT) calculations and experimental nuclear magnetic resonance spectra for glycine adsorption at silica surfaces, highlighting the importance of H-bonds with oxide surface for the adsorption (*44*, *45*). Such orientational constraints help the formation of stable assembly states and have been observed in the crystal structures of small molecules (*46*, *47*). H-bonds between amino acids and surface are expected to stabilize the transition states in the condensation reactions.

The second valley at $Z = 0.4$ and 0.5 nm represents configurations in which only the N terminus or C terminus of the molecule is H-bonded with the surface, but not both. This valley of the GG dipeptide is wider and deeper than that of glycine, indicating that the GG dipeptide is more likely to be perpendicular to the surface (Fig. 2, D, F, H, and J). Such configurations are essential for surface-catalyzed peptide formation because the newly formed peptide bond is moved away from the surface to avoid hydrolysis. In addition, by freeing space on the surface, reaction products do not competitively inhibit binding of additional reactants.

To characterize the orientational propensity of the bound configurations, we calculated a 2D FES by complementing the distance from the surface, Z, with a second CV, θ_{NC} (Fig. 2, G and H), and reweighting molecular configurations along the biased trajectory before computing the histograms. The affinity of N-terminal adsorption is higher than that of C-terminal adsorption by several k_BT, which is consistent with previous reported results that positive ions have stronger affinity than negative ions (*39*). For pure water, at the α-alumina/water interface, water donates stronger H-bonds to the surface and accepts weaker H-bonds from surface OH groups at neutral surface in neutral solutions, i.e., pH 7 (*48*, *49*). N-adsorption can also attract protons of the amine groups, increasing its nucleophilicity, although quantitatively estimating proton affinity to amine groups or surface OH groups is difficult because the pK_a (where K_a is the acid dissociation constant) of surface OH groups (*50*) and how the interfacial environment affects water's pK_a (*51*–*53*) are still unclear. Despite this uncertainty to proton affinity, the adsorption configurations observed in our simulations support a promising picture of surface-induced amino acid condensation reactions at the α-alumina(0001) surface.

Adsorption and interaction of multiple glycine molecules

Amino acid condensation reactions cannot occur with a single glycine molecule. To investigate interactions between amino acids at the alumina surface, we conducted unbiased MD simulations containing 20 glycine molecules on each side of alumina surfaces. When multiple glycine molecules are present, they accumulate at the interface. On average, 15 molecules adsorb at the surface, leading to a higher local number density than that in the bulk, in agreement with the adsorption free energy of a single glycine molecule discussed above. What is more, the higher glycine concentration at the surface further increases the affinity of glycine for the surface by an additional 2 k_BT (fig. S4), indicating that there are interactions between glycine molecules that pull glycine from the bulk to the surface. Although the dynamics of glycine adsorption is beyond the scope of the work, glycine molecules need to stay adsorbed for a certain period of time to be catalyzed in the condensation reaction. Our simulations show that on average the residence time for glycine is 65 ns, with some molecules staying adsorbed for up to 100 ns (fig. S6). Since the total unbiased simulation time is only 100 ns, the actual residence time could be longer.

The pattern of adsorbed glycine monomers in simulations shows that they are not isolated at the alumina surface; instead, they can form long chains via H-bonds between the carboxyl and amine groups of two glycine monomers (Fig. 3A). Our hypothesis is that such configurations are the precursors to peptides because there are many contact amino acid pairs, which enhance the possibility of the condensation reactions and the formation of long peptide chains. To investigate the pattern of adsorbed glycine monomers, we carried

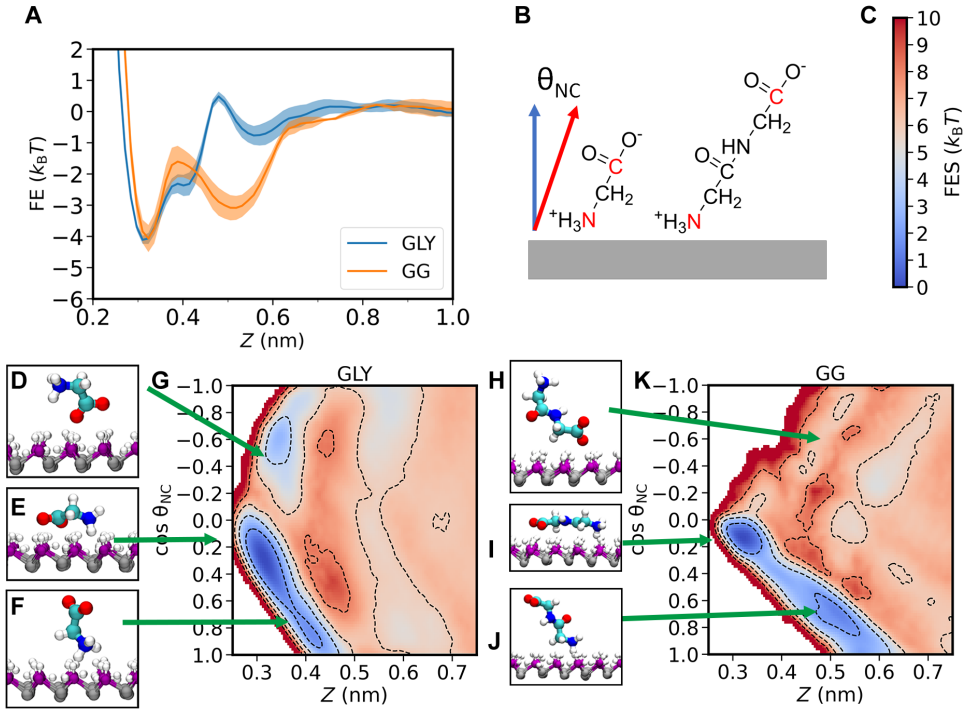

Fig. 2. Simulation results of single amino acid adsorption. (**A**) 1D FES of the adsorption of a single molecule, glycine, and GG dipeptide. The free energy in the bulk is set to 0. (**B**) Atomic structure of a glycine (left) and GG dipeptide (right) molecule. The gray rectangle below the molecules represents the alumina surface. (**C**) Color bar for 2D FES plots (G) and (K). (**D** to **F**) Snapshots of C-adsorption, flat-adsorption, and N-adsorption of a glycine on the α-alumina(0001) surface. (**H** to **J**) Snapshots of (H) C-adsorption, (I) flat-adsorption, and (J) N-adsorption of a GG dipeptide. (**G** and **K**) 2D FES of glycine and GG dipeptide adsorption; arrows mark the CVs of FES for different adsorption configurations. Snapshot color code: gray, aluminum; purple, surface oxygen; white, hydrogen; blue, nitrogen; cyan, carbon; red, nonsurface oxygen. Water is not shown in the snapshots for better visualization.

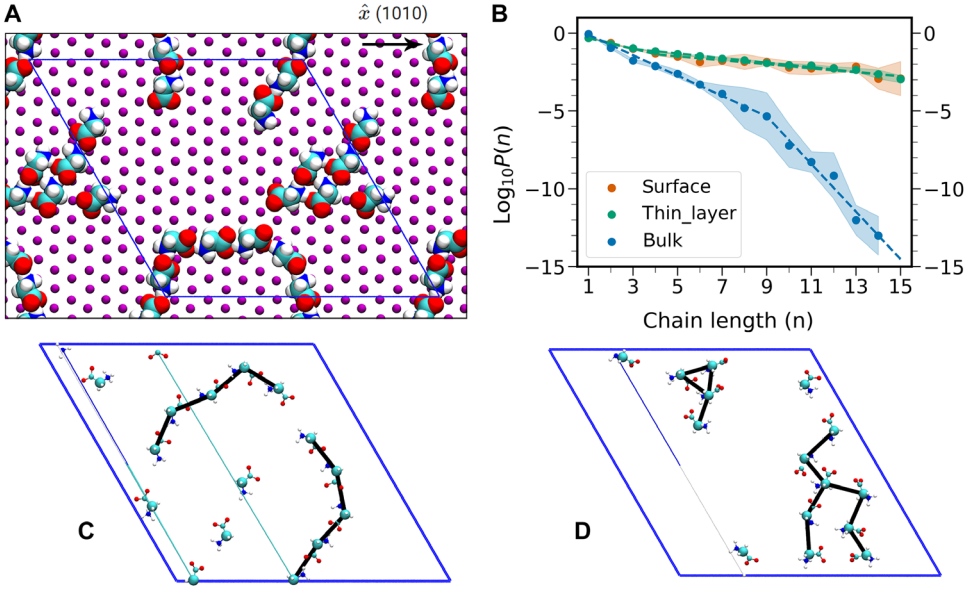

Fig. 3. Simulation results in the presence of multiple glycine monomers. (**A**) Snapshot from the simulation. (**B**) Probability distribution of the length of glycine chain (*n*) in different simulations. Each dot represents mean results from simulations, and lines are fits to the mean results. Shaded area on each dot represents the error bar, defined by one SD of *P*(*n*) at each *n*. Red, green, and blue colors represent surface, thin_layer, and bulk, respectively. (**C** and **D**) Snapshots illustrating how glycine connections and chain lengths are determined. The large cyan atoms represent Cα atoms, and black lines indicate that two glycine molecules are connected when the distance between their Cα atoms is less than 0.64 nm.

out metadynamics simulations, biasing the average coordination number ($\overline{CN}$) and Coulomb energy (U_E) of adsorbed glycine (additional details are discussed in the Supplementary Materials) (*40*, *54*). When visualizing the trajectories of metadynamics simulations, we observed transitions among isolated adsorbed glycine monomers that do not contact with others, linear chains, and clusters (Fig. 4). This indicates that biasing $\overline{CN}$ and U_E, CVs that are simple to implement, can efficiently lead to transitions between aggregation and isolation of adsorbed glycine, although they may not be the best CVs to drive phase transitions (*47*, *54*). We use reweighting (*43*) to compute the probability as a function of the length of an assembled glycine chain (n) to quantify the structure of glycine aggregates. A similar CV was applied to study the solid-liquid phase transition of NaCl (*55*). Two glycine molecules are counted as connected if the distance of their Cα atoms is less than 0.64 nm. n represents the number of connected glycines (Fig. 3, C and D). For instance, Fig. 3C contains five isolated glycines ($n = 1$), two chains with length $n = 5$. Figure 3D contains three isolated glycines, two chains with length $n = 4$ (top) and $n = 8$ (right).

Our simulation results do not exactly match the Flory model of polymerization, which predicts that the number density of longer chains decays exponentially with the chain length. We proposed a two-segment model, based on the Flory model to mimic the auto-catalysis or co-polymerization mechanisms (*10*, *56*). The details of the fitting procedure is discussed in the Supplementary Materials (section S4.3, eqs. S8 to S11). In short, when the length of glycine chains is longer than a critical length (defined as s), a change of the Flory P value is included in the model. Comparing the chain length probability distribution, $P(n)$, between simulations of surface and bulk (Fig. 3B), at $n = 10$, $P(n=10)$ for surface (10^{-2}) is at least five orders of magnitude larger than that in the bulk (10^{-7}). Such notable enhancement of self-assembly of glycine shows the necessity of the oxide surface to promote the aggregation of glycine. In addition, the behavior of surface and bulk for chains that are longer than the critical length ($n > s$) is the opposite: $p_2 > p_1$ is observed at the surface, but $p_2 < p_1$ in the bulk. The former is attributed to the auto-catalysis or co-polymerization mechanisms as discussed above, while the latter is due to depletion. When large glycine clusters form from aqueous solutions, phase separation occurs, decreasing the glycine density in the liquid phase, which increased the free energy required for the growth of the cluster (*54*, *55*).

Here, we observed these patterns for adsorbed glycine molecules: isolated, linear chain, and cluster (Fig. 4). In the isolated pattern, glycine moieties do not contact each other and thus do not form aggregates. However, due to the definition of continuous CN, the corresponding CN value is greater than zero, even in the absence of contacts. The linear chain pattern refers to connected glycine moieties each donating H-bonds from its N terminus and accepting H-bonds at its C terminus. A perfect linear chain is expected to be characterized by $\overline{CN} = 2$ with fluctuations due to branching defects. The cluster pattern can be either amorphous or ordered. We observed anti-parallel two-strand chains, similar to the α-glycine solid structure (Fig. 4C) (*47*). Although the detailed phases of glycine on a surface are not the topic of the manuscript, simulation results show that adsorption of glycine on the surface promotes the formation of solid-like aggregated states. However, in solution, the dissolved states are greatly favored, consistent with other published reports (*31*, *40*).

We also compare the growth of glycine clusters with classical nucleation theory (CNT). For simulations of both surface and bulk, we observed a free energy increase during growth. We do not observe a critical radius and a decrease of free energy during the growth of larger clusters. Such observation is beyond what CNT predicted, but still reasonable because (i) the number of glycines is too few and may be smaller than the critical size; (ii) the depletion reduces the stability of the solid phase, and to overcome it, the constant chemical potential simulations are necessary to maintain the concentration of glycine in the solution (*55*); (iii) the shape of molecules is ignored in CNT, but the growth of glycine clusters is anisotropic: forming linear chains, cluster with anti-parallel strands (similar to the solid α-glycine), and parallel strands (similar to the solid γ-glycine). We believe that the behavior of glycine assembly is expected to be between the Flory model and CNT. The critical size for clusters predicted by CNT is too large to form in dilute aqueous solutions; however, before reaching that point, there is a subcritical point that requires less free energy for the growth of glycine clusters before reaching the critical size, equivalent to the observation of self-acceleration ($p_2 > p_1$) mechanism.

To investigate how glycine local density and the 2D nature of adsorbed glycine affect the chain growth, we designed additional simulations without alumina surface, but all glycine molecules are restrained within a thin layer (fig. S2) with a glycine density comparable to that observed at the surface (fig. S7). Metadynamics results show that their $P(n)$ and FES (fig. S9) are also similar (Fig. 3B), indicating that the primary role of the surface in promoting the assembly of glycine is to enhance the local glycine density. We notice that the error bar of $P(n)$ for the thin_layer is relatively smaller than that for surface, because of much better sampling. Such observation is mainly due to the slow dynamics of glycine at the alumina surface.

The high density of glycine at the surface arises from strong interactions between glycine and the alumina surface, and these strong interactions lead to the slow dynamics of glycine on the surface (*48*). Slow dynamics make sampling difficult, and large errors in $P(n)$ result for high n. A sharp decrease of $P(n=14)$ and $P(n=15)$

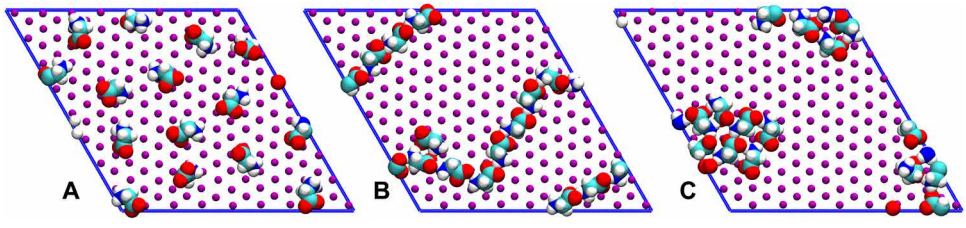

Fig. 4. Snapshots of patterns of adsorbed glycine molecules on the alumina surface. Only the surface oxygen atoms are shown (purple). Blue lines represent the boundary of the simulation box. (**A** to **C**) Isolated, linear chain, and cluster pattern, respectively.

could lead to the underestimation of the Flory probability after the critical size, p_2.

When examining each independent simulations, in one replica, $P(n=14)$ and $P(n=15)$ are notably lower than other runs (fig. S12). Despite such possible underestimation, p_2 of the surface is still higher than that of the bulk (Table 1); that is, at the surface, the decay of probability to observe long chains is slower, indicating that surface is necessary for chains longer than 15 or 20 to form. This slow decay of $P(n)$ with n at the surface suggests that interactions with surfaces can also notably contribute to the growth of glycine assemblies, especially for long chains.

Upon adsorption, the structure of the surface induces the formation of ordered glycine patterns. We first examine the azimuthal orientation (ϕ) of adsorbed glycine molecules, defined by the angle between the projection of **NC** vector onto the surface and $\hat{x}$, the $(10\bar{1}0)$ direction of the surface. The vector of a glycine is $\mathbf{NC} = (x_{NC}, y_{NC}, z_{NC})$, and ϕ is the angle between vectors (x_{NC}, y_{NC}) and $(1, 0)$ in the counterclockwise direction. We calculated $P(\phi)$ without reweighting the metadynamics because reweighting may overweight certain structures and make it difficult to evaluate the overall sampled configurations. In simulations of thin_layer, there is no surface to align glycine molecules and there is no preferred orientations. However, the hexagonal structure of alumina affects orientations. We calculate $P(\phi \mid n)$, the probability of glycine orientation when it belongs to a chain with length n, to combine the information of glycine orientation and chain length. For isolated adsorbed glycine, $P(\phi \mid n=1)$ shows six peaks following the direction of surface oxygen atoms (Fig. 5A). In addition, although not well sampled, the surface also leads to preferred values of $\phi \approx 90°$, 210°, and 330°, which may be induced by the orientations of in-plane surface OH groups, similar to the adsorption of pure water (*48*). As the glycine chain length grows, $P(\phi)$ becomes more uneven, indicating that long chains have a stronger preference for certain orientations. In other words, surface structures align the orientation of adsorbed glycine, and such alignment effect is stronger in longer glycine chains.

Another effect of alumina surfaces is the specific position of adsorption. Adsorbed glycine molecules are not homogeneously distributed on the surface but prefer to be adsorbed at the triangular sites formed by three surface aluminol groups. The number density of carboxyl oxygens and amine nitrogens is notably lower outside these triangular sites (Fig. 6, E and F). The carboxyl oxygen atoms are positioned on top of one or between two surface oxygen atoms, accepting one or two H-bonds from aluminol groups (Fig. 6, A and B). Amine nitrogens prefer to be in the center of triangular sites but usually do not donate all three H-bonds to aluminol groups (Fig. 6, C and D). These configurations are geometrically similar to those observed in the adsorption of simple ions, such as F^- and Na^+ (*39*, *48*), because amine and carboxyl groups contain negative and positive charges, respectively. Such surface-templated adsorption promotes ordered patterns of adsorbed glycines, limiting their motion and facilitating the formation of extended glycine chains. When glycine molecules are absent, interfacial waters strongly H-bond with the surface (*48*), but adsorbed glycines lose part of their own hydration shells and replace those surface-bound waters. As a result, the electrostatic interactions between glycine and the surface must be strong enough to compensate for the loss of interfacial water.

Role of water during glycine adsorption

Since water is present in the glycine solution and contacts the alumina surface, its role during the growth of glycine chains should not be ignored. Because of the difficulty of calculating high dimensional

Table 1. Fitting results from metadynamics simulations biasing $\overline{CN}$ and U_E. The parameters k and s are obtained from fitting as discussed in the Supplementary Materials. The probability p in the Flory model in Eq. 1 is given by $p = e^k$. s represents the critical chain length, where p_2 is different from p_1 due to self-assembly for surface and thin_layer, or depletion in the bulk.

	k_1	p_1	k_2	p_2	s
Surface	−0.82	0.43	−0.30	0.74	4
Thin_layer	−0.79	0.46	−0.34	0.71	3
Bulk	−1.51	0.22	−3.52	0.03	9

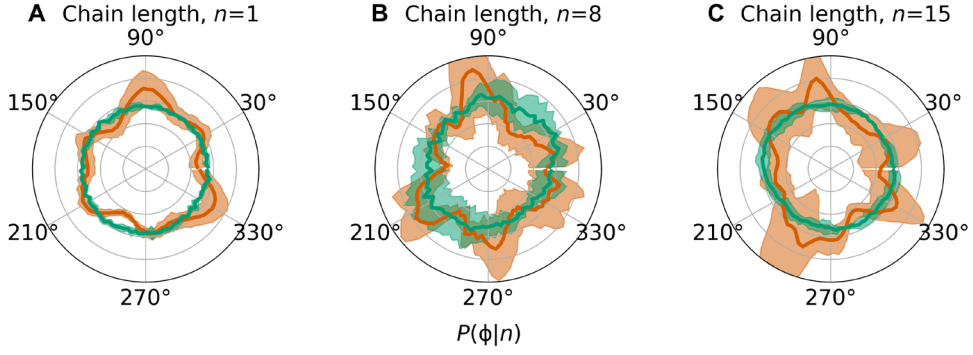

Fig. 5. Probability distribution of a glycine molecule's azimuthal orientation (ϕ) given a certain length of chain (n) it belongs to. (**A**, **B**, and **C**) represent chain lengths of n = 1, 8, and 15, respectively. The red and green curves are calculated from metadynamics simulations of surface and thin_layer, respectively. Shaded areas represent the error bar, defined as one standard deviation. Completed plots for n = 1 to 15 are provided in fig. S13.

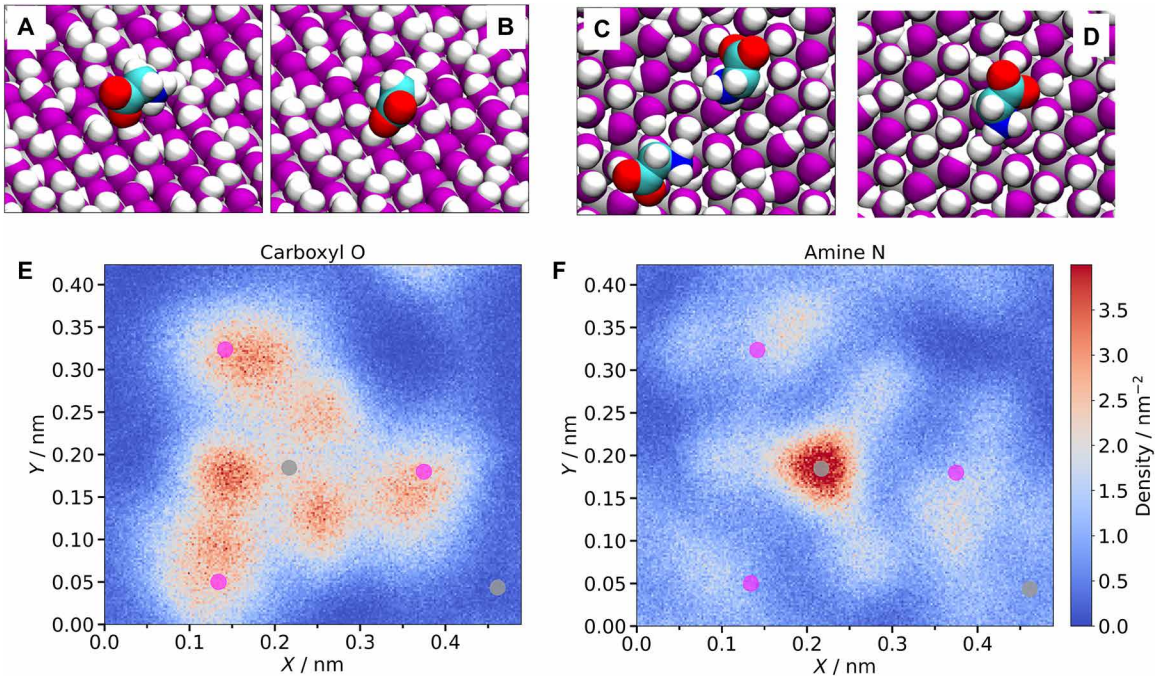

Fig. 6. Interaction between adsorbed glycine with surface aluminol groups. In the snapshots, glycine can accept one (**A**) or two (**B**) H-bonds from AlOH groups using its carboxyl group, or donate one [(**C**), bottom], two [(C), top], or three (**D**) H-bonds using its amine group. (**E** and **F**) 2D density distribution of carboxyl carbon (E) and amine nitrogen (F) atoms at the α-alumina(0001) surface within a unit cell. Purple and gray dots in the plots represent surface oxygen and aluminum atoms, respectively.

FES, water is not included in the CVs in metadynamics simulations. However, previous studies have shown that water plays a critical role in the nucleation of NaCl from aqueous solution (*40*, *55*). Moreover, committor analysis has revealed that water is the reaction barrier of ion pairing in aqueous solutions (*57*, *58*), suggesting the necessity of water removal during the growth of glycine chains.

To quantify contributions from water to glycine assembly growth, we calculate the probability distribution of coordination number of water (CN_{Ow}) and surface aluminal AlOH groups (CN_{Os}) for each glycine in a chain of a given length [$P(CN_{Ow} + CN_{Os} \mid n)$], as shown in Fig. 7. Surface oxygen can also coordinate with glycine and $CN_{Os} = 0$ in simulations thin_layer and bulk. Water and surface is considered coordinated if its oxygen is within 0.35 nm of the amine nitrogen or carboxyl oxygen atoms.

The metadynamics trajectories are treated as unbiased without any reweighting. In all three environments, surface, thin_layer, and bulk, isolated glycine ($n = 1$) has the highest coordinated water except for some n values, likely due to the limited sampling of configurations. As chains grow, the average water CN of all glycine ($\overline{CN_{Ow} + CN_{Os}}$) decreases, indicating that glycine assembly requires the removal of water. On average, each glycine needs to remove three or four water molecules as chain lengths increase to $n = 15$ from isolated. This observation could explain why the alumina templating effects do not notably aid the assembly of glycine: The hydrophilic surface hinders water removal (*48*). The oxygen coordination contributed by AlOH (CN_{Os}) does not change with n, indicating that the removal of water (CN_{Ow}) but not aluminol affects the assembly of glycine monomers (fig. S14).

Finally, $P(CN_{Ow} + CN_{Os})$ and $\overline{CN_{Ow} + CN_{Os}}$ estimate the contribution of water during glycine chain formation. The most important

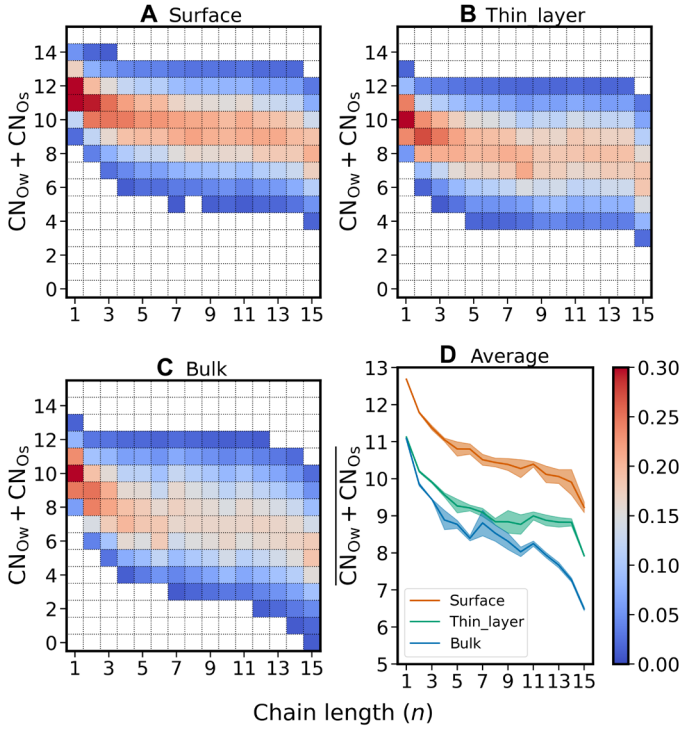

Fig. 7. Correlation between water and glycine chain length. (**A** to **C**) Probability distribution of water and surface oxygen coordinated number of a glycine in a chain of given length n [$P(CN_{Ow} + CN_{Os} \mid n)$]. CN_{Os} is 0 for plots (B) and (C). For clarity, the grids are white if $P(CN_{Ow} + CN_{Os}) < 0.01$. (**D**) Average coordinated water for glycine in chain length n. Shades represent the error bar, one standard deviation.

factor is expected to be the behavior of the bridge water molecules, defined as water that connects with more than one glycine chain (*57*, *58*). To investigate the behavior of those bridge water molecules, additional simulations with CVs including their contribution are necessary. Proper dimension reduction of CVs is needed in future works.

DISCUSSION

Previous DFT calculations have demonstrated that at silica surfaces, surface OH groups facilitate amino acid condensation reactions by assisting proton transfer or stabilizing charged species during the reaction (*59*, *60*). Despite their critical role, these processes are challenging to investigate due to the limited understanding of the proton affinity of alumina(0001) surfaces. Two possible proton transfer processes could occur: $AlOH \rightleftharpoons AlO^- + H^+$ (pK_{a1}) and $AlOH_2^+ \rightleftharpoons AlOH + H^+$ (pK_{a2}). pK_{a2} is predicted to be approximately 0 based on both DFT-MD simulations and experimental measurements, while estimates for pK_{a1} range from 13 to 22. A low pK_{a1} suggests that the alumina(0001) surface exhibits a comparable propensity to adsorb and release protons, aligning with most experimental observations (*50*, *61*, *62*). Conversely, a high predicted pK_{a1} implies that rendering the surface negatively charged is extremely difficult, as observed in most MD simulations (*50*, *63*, *64*).

Although this issue lies outside the scope of this work, accurately determining the pK_a of alumina and exploring its impact on glycine adsorption at the DFT level would aid in developing future models. Given that this study employs classical MD simulations, modeling proton transfer and pH effects on surface protonation states remains a great challenge. For simplicity, we assume a neutral solution without additional H^+ or OH^- at pH 7, and a neutral charged alumina surface, consistent with previously reported pK_{a1} and pK_{a2} values.

To explain why $P(n)$, the probability of long chains, and p, the Flory probability, are similar for the surface and thin layer despite strong interactions between glycine and the surface, we propose a competition between enthalpy and entropy. Glycine adsorption, driven by electrostatic interactions, is enthalpy-favored. However, the strong interactions restrict the position and orientation of adsorbed glycine molecules, resulting in an entropy penalty (*40*, *65*). The similarity in $P(n)$ and p suggests that the enthalpy and entropy effects offset each other at the alumina surface. Nonetheless, the higher p_2 observed for the surface compared to the thin layer indicates that, in addition to the higher local concentration, the templating effects of the alumina surface contribute to the self-assembly of H-bonded glycine chains.

Finally, the role of water in amino acid condensation reactions warrants further investigation. Under dry conditions, increasing the temperature promotes the reaction by removing by-product water (*19*). Previous studies emphasize the importance of wetting-drying cycles in amino acid adsorption (*8*). These findings, supported by experiments and MD simulations, underscore the need to quantify water's role during the reaction. However, modeling the slow, out-of-equilibrium wetting-drying cycle is challenging and requires carefully designed enhanced sampling MD simulations. Here, we focus on the correlation between the removal of bridging water and the aggregation of adsorbed glycine, using the CV for the number of bridging water molecules. While this CV may not fully capture water-glycine interactions (*40*), additional CVs involving solvent water are needed. Machine learning–based MD simulations and data analysis could provide deeper insights into the role of water (*47*).

Here, using classical MD simulations with metadynamics, an enhanced sampling technique, we studied glycine adsorption and assembly at the water/α-alumina(0001) interface. Simulations reveal how the solid surface promotes the adsorption and self-assembly of glycine, as a model of amino acid polymerization, a crucial step in forming bioactive molecules from abiotic building blocks. The amine and carboxyl groups of glycine and GG dipeptide can form H-bonds with the surface, showing an affinity of about $4\,k_BT$, thereby increasing the local density of glycine. Adsorbed glycine can interact with each other via H-bonds and form long glycine chains. These long chains have stable structures with slow dynamics, increasing the probability for glycine to contact and undergo condensation reactions. By fitting to a modified Flory model, we find that the probability of forming a chain with 10 glycine molecules is at least 10^5 times higher at the surface than in bulk water. Our findings show that adsorbed glycine at the alumina surface prefers specific surface sites and adopts preferred orientations following the lattice direction of surface oxygen atoms, particularly in long chains with high n. Water also plays an important role. Glycine in long chains has fewer coordinated water molecules than it does as an isolated monomer in solution, indicating the necessity of water removal to form long chains during the assembly of adsorbed glycine. Although questions pertaining to the thermodynamics and kinetics of interfacial peptide condensation reactions necessitate further investigations using quantum mechanical approaches, this work reveals how oxide surfaces promote pre-reaction assembly and accelerate the prebiotic formation of life's building blocks because of high local density and surface templating effects.

MATERIALS AND METHODS

The alumina configuration is described by Lutterotti and Scardi (*66*). The simulation box is hexagonal with $a = b \approx 3.9$ nm, $c = 40$ nm, $\alpha = \beta = 90°$, and $\gamma = 120°$, containing 8×8 unit cells (fig. S1, A and D). Similar to our previous work (*39*), the α-alumina(0001) surface is covered by aluminol (Al-O-H) groups with the C3 symmetry (fig. S8B) and is set in the middle of the simulation box with a thickness of about 4 nm. Both sides of the alumina were OH-terminated and contain water with a thickness of about 10 nm on each side. The vacuums on both sides are about 9 nm thick to maintain the simulation at the pressure of water-vapor coexistence. In unbiased simulations, there are 8062 water molecules and 20 glycine molecules on each side, making the initial bulk concentration of glycine 0.28 M. Motion propagation is calculated using the leapfrog algorithm. The oxide structure in all simulations is fully flexible. In the production runs, the $NP_{xy}L_zT$ ensemble is applied, that is, constant pressure is maintained in the X and Y directions at 1 bar using the Parrinello-Rahman barostat (*67*, *68*), and the length of the simulation box perpendicular to the alumina surface (Z) is fixed. The temperature is maintained at 300 K using the velocity rescaling with a relaxation time of 0.1 ps (*69*). Water bond lengths and bond angles are fixed using the LINCS algorithm (*70*). Short-range interactions are cut off at 1 nm. Long-range electrostatics are evaluated with the particle-mesh Ewald method. The simulation time of unbiased simulation is 100 ns (*71*).

The zwitterion forms of glycine and the GG dipeptide are used in this work (fig. S1C). The CHARMM27 force field is applied to amino acids (*72*, *73*). The ClayFF force field (*74*) and the SPC/E model (*75*) are used for the alumina and water, respectively.

All MD simulations are carried out using the GROMACS 2016.3 package (*76*) with PLUMED 2.3 (*77*). Files of GROMACS and PLUMED are available at https://github.com/ruiyuwangwork/GLY_Alumina. Additional details for metadynamics, including implementation of CVs, are described in the Supplementary Materials.

Supplementary Materials

This PDF file includes:

Supplementary Text
Figs. S1 to S14
References

REFERENCES AND NOTES

1. J. D. Bernal, The physical basis of life. *Proc. Phys. Soc. B* **62**, 597 (1949).
2. J. P. Ferris, A. R. Hill Jr., R. Liu, L. E. Orgel, Synthesis of long prebiotic oligomers on mineral surfaces. *Nature* **381**, 59–61 (1996).
3. L. E. Orgel, Polymerization on the rocks: Theoretical introduction. *Orig. Life Evol. Biosph.* **28**, 227–234 (1998).
4. C. Kocher, K. A. Dill, Origins of life: First came evolutionary dynamics. *QRB Discov.* **4**, e4 (2023).
5. A. M. Garcia, D. Iglesias, E. Parisi, K. E. Styan, L. J. Waddington, C. Deganutti, R. De Zorzi, M. Grassi, M. Melchionna, A. V. Vargiu, S. Marchesan, Chirality effects on peptide self-assembly unraveled from molecules to materials. *Chem* **4**, 1862–1876 (2018).
6. A. M. Garcia, M. Melchionna, O. Bellotto, S. Kralj, S. Semeraro, E. Parisi, D. Iglesias, P. D'Andrea, R. De Zorzi, A. V. Vargiu, S. Marchesan, Nanoscale assembly of functional peptides with divergent programming elements. *ACS Nano* **15**, 3015–3025 (2021).
7. I. Budin, J. W. Szostak, Expanding roles for diverse physical phenomena during the origin of life. *Annu. Rev. Biophys.* **39**, 245–263 (2010).
8. V. Erastova, M. T. Degiacomi, D. Fraser, H. C. Greenwell, Mineral surface chemistry control for origin of prebiotic peptides. *Nat. Commun.* **8**, 2033 (2017).
9. S. A. Benner, A. Ricardo, M. A. Carrigan, Is there a common chemical model for life in the universe? *Curr. Opin. Chem. Biol.* **8**, 672–689 (2004).
10. E. Guseva, R. N. Zuckermann, K. A. Dill, Foldamer hypothesis for the growth and sequence differentiation of prebiotic polymers. *Proc. Natl. Acad. Sci. U.S.A* **114**, E7460–E7468 (2017).
11. S. L. Miller, A production of amino acids under possible primitive earth conditions. *Science* **117**, 528–529 (1953).
12. A. M. Saitta, F. Saija, Miller experiments in atomistic computer simulations. *Proc. Natl. Acad. Sci. U.S.A* **111**, 13768–13773 (2014).
13. E. Schreiner, N. N. Nair, D. Marx, Peptide synthesis in aqueous environments: The role of extreme conditions on peptide bond formation and peptide hydrolysis. *J. Am. Chem. Soc.* **131**, 13668–13675 (2009).
14. T. M. McCollom, Miller-Urey and beyond: What have we learned about prebiotic organic synthesis reactions in the past 60 years? *Annu. Rev. Earth Planet. Sci.* **41**, 207–229 (2013).
15. A. Pérez-Villa, F. Pietrucci, A. M. Saitta, Prebiotic chemistry and origins of life research with atomistic computer simulations. *Phys. Life Rev.* **34-35**, 105–135 (2020).
16. W. H. Stockmayer, Molecular distribution in condensation polymers. *J. Polym. Sci.* **9**, 69–71 (1952).
17. P. J. Flory, Molecular size distribution in linear condensation polymers. *J. Am. Chem. Soc.* **58**, 1877–1885 (1936).
18. E. L. Shock, Stability of peptides in high-temperature aqueous solutions. *Geochim. Cosmochim. Acta* **56**, 3481–3491 (1992).
19. K. Marshall-Bowman, S. Ohara, D. A. Sverjensky, R. M. Hazen, H. J. Cleaves, Catalytic peptide hydrolysis by mineral surface: Implications for prebiotic chemistry. *Geochim. Cosmochim. Acta* **74**, 5852–5861 (2010).
20. W. Martin, J. Baross, D. Kelley, M. J. Russell, Hydrothermal vents and the origin of life. *Nat. Rev. Microbiol.* **6**, 805–814 (2008).
21. B. Yang, K. Niu, F. Haag, N. Cao, J. Zhang, H. Zhang, Q. Li, F. Allegretti, J. Björk, J. V. Barth, L. Chi, Abiotic formation of an amide bond via surface-supported direct carboxyl-amine coupling. *Angew. Chem. Int. Ed. Engl.* **61**, e202113590 (2022).
22. E. Schreiner, N. N. Nair, C. Wittekindt, D. Marx, Peptide synthesis in aqueous environments: The role of extreme conditions and pyrite mineral surfaces on formation and hydrolysis of peptides. *J. Am. Chem. Soc.* **133**, 8216–8226 (2011).
23. J.-F. Lambert, M. Jaber, T. Georgelin, L. Stievano, A comparative study of the catalysis of peptide bond formation by oxide surfaces. *Phys. Chem. Chem. Phys.* **15**, 13371–13380 (2013).
24. R. M. Hazen, D. A. Sverjensky, Mineral surfaces, geochemical complexities, and the origins of life. *Cold Spring Harb. Perspect. Biol.* **2**, a002162 (2010).
25. H. James Cleaves II, A. M. Scott, F. C. Hill, J. Leszczynski, N. Sahai, R. Hazen, Mineral-organic interfacial processes: Potential roles in the origins of life. *Chem. Soc. Rev.* **41**, 5502–5525 (2012).
26. B. Grégoire, V. Erastova, D. L. Geatches, S. J. Clark, H. C. Greenwell, D. G. Fraser, Insights into the behaviour of biomolecules on the early Earth: The concentration of aspartate by layered double hydroxide minerals. *Geochim. Cosmochim. Acta* **176**, 239–258 (2016).
27. J.-F. Lambert, Adsorption and polymerization of amino acids on mineral surfaces: A review. *Orig. Life Evol. Biosph.* **38**, 211–242 (2008).
28. A. D. McKee, M. Solano, A. Saydjari, C. J. Bennett, N. V. Hud, T. M. Orlando, A possible path to prebiotic peptides involving silica and hydroxy acid-mediated amide bond formation. *Chembiochem* **19**, 1913–1917 (2018).
29. N. Kitadai, H. Oonishi, K. Umemoto, T. Usui, K. Fukushi, S. Nakashima, Glycine polymerization on oxide minerals. *Orig. Life Evol. Biosph.* **47**, 123–143 (2017).
30. S. S. Lee, A. Koishi, I. C. Bourg, P. Fenter, Ion correlations drive charge overscreening and heterogeneous nucleation at solid-aqueous electrolyte interfaces. *Proc. Natl. Acad. Sci. U.S.A* **118**, e2105154118 (2021).
31. W. Zhao, Y. Sun, W. Zhu, J. Jiang, X. Zhao, D. Lin, W. Xu, X. Duan, J. S. Francisco, X. C. Zeng, Two-dimensional monolayer salt nanostructures can spontaneously aggregate rather than dissolve in dilute aqueous solutions. *Nat. Commun.* **12**, 5602 (2021).
32. F. S. Brigiano, M. Gierada, F. Tielens, F. Pietrucci, Mechanism and free-energy landscape of peptide bond formation at the silica-water interface. *ACS Catal.* **12**, 2821–2830 (2022).
33. L. Grill, S. Hecht, Covalent on-surface polymerization. *Nat. Chem.* **12**, 115–130 (2020).
34. J. Adisoejoso, Y. Li, J. Liu, P. N. Liu, N. Lin, Two-dimensional metallo-supramolecular polymerization: Toward size-controlled multi-strand polymers. *J. Am. Chem. Soc.* **134**, 18526–18529 (2012).
35. D. Deamer, S. Singaram, S. Rajamani, V. Kompanichenko, S. Guggenheim, Self-assembly processes in the prebiotic environment. *Philos. Trans. R. Soc. Lond. B Biol. Sci.* **361**, 1809–1818 (2006).
36. J. B. Awuah, T. R. Walsh, Side-chain effects on the co-existence of emergent nanopatterns in amino acid adlayers on graphene. *Nanoscale* **12**, 13662–13673 (2020).
37. J. B. Awuah, T. R. Walsh, Predictions of pattern formation in amino acid adlayers at the in vacuo graphene interface: Influence of termination state. *Small* **16**, e1903403 (2020).
38. M. J. DelloStritto, S. M. Piontek, M. L. Klein, E. Borguet, Effect of functional and electron correlation on the structure and spectroscopy of the Al_2O_3(001)-H_2O interface. *J. Phys. Chem. Lett.* **10**, 2031–2036 (2019).
39. R. Wang, M. DelloStritto, R. C. Remsing, V. Carnevale, M. L. Klein, E. Borguet, Sodium halide adsorption and water structure at the α-alumina(0001)/water interface. *J. Phys. Chem. C* **123**, 15618–15628 (2019).
40. R. Wang, P. Tiwary, Atomic scale insights into NaCl nucleation in nanoconfined environments. *Chem. Sci.* **15**, 15391–15398 (2024).
41. A. Barducci, G. Bussi, M. Parrinello, Well-tempered metadynamics: A smoothly converging and tunable free-energy method. *Phys. Rev. Lett.* **100**, 020603 (2008).
42. A. Laio, M. Parrinello, Escaping free-energy minima. *Proc. Natl. Acad. Sci. U.S.A* **99**, 12562–12566 (2002).
43. P. Tiwary, M. Parrinello, A time-independent free energy estimator for metadynamics. *J. Phys. Chem. B* **119**, 736–742 (2015).
44. N. Folliet, C. Gervais, D. Costa, G. Laurent, F. Babonneau, L. Stievano, J.-F. Lambert, F. Tielens, A molecular picture of the adsorption of glycine in mesoporous silica through NMR experiments combined with DFT-D calculations. *J. Phys. Chem. C* **117**, 4104–4114 (2013).
45. H. Abadian, P. Cornette, D. Costa, A. Mezzetti, C. Gervais, J.-F. Lambert, Leucine on silica: A combined experimental and modeling study of a system relevant for origins of life, and the role of water coadsorption. *Langmuir* **38**, 8038–8053 (2022).
46. P. M. Piaggi, M. Parrinello, Predicting polymorphism in molecular crystals using orientational entropy. *Proc. Natl. Acad. Sci. U.S.A.* **115**, 10251–10256 (2018).
47. Z. Zou, E. R. Beyerle, S.-T. Tsai, P. Tiwary, Driving and characterizing nucleation of urea and glycine polymorphs in water. *Proc. Natl. Acad. Sci. U.S.A.* **120**, e2216099120 (2023).
48. R. Wang, Y. Zou, R. C. Remsing, N. O. Ross, M. L. Klein, V. Carnevale, E. Borguet, Superhydrophilicity of α-alumina surfaces results from tight binding of interfacial waters to specific aluminols. *J. Colloid Interface Sci.* **628**, 943–954 (2022).
49. X. Du, W. Shao, C. Bao, L. Zhang, J. Cheng, F. Tang, Revealing the molecular structures of α-Al2O3 (0001)–water interface by machine learning based computational vibrational spectroscopy. *J. Chem. Phys.* **161**, 124702 (2024).
50. R. Wang, M. L. Klein, V. Carnevale, E. Borguet, Investigations of water/oxide interfaces by molecular dynamics simulations. *WIREs Comput. Mol. Sci.* **11**, e1537 (2021).
51. M. D. Baer, I. F. W. Kuo, D. J. Tobias, C. J. Mundy, Toward a unified picture of the water self-ions at the air-water interface: A density functional theory perspective. *J. Phys. Chem. B* **118**, 8364–8372 (2014).

52. F. Giberti, A. A. Hassanali, The excess proton at the air-water interface: The role of instantaneous liquid interfaces. *J. Chem. Phys.* **146**, 244703 (2017).
53. A. Tuladhar, S. M. Piontek, E. Borguet, Insights on interfacial structure, dynamics, and proton transfer from ultrafast vibrational sum frequency generation spectroscopy of the alumina(0001)/water interface. *J. Phys. Chem. C* **121**, 5168–5177 (2017).
54. R. Wang, S. Mehdi, Z. Zou, P. Tiwary, Is the local ion density sufficient to drive NaCl nucleation from the melt and aqueous solution? *J. Phys. Chem. B* **128**, 1012–1021 (2024).
55. T. Karmakar, P. M. Piaggi, M. Parrinello, Molecular dynamics simulations of crystal nucleation from solution at constant chemical potential. *J. Chem. Theory Comput* **15**, 6923–6930 (2019).
56. R. F. Goldstein, L. Stryer, Cooperative polymerization reactions. Analytical approximations, numerical examples, and experimental strategy. *Biophys. J.* **50**, 583–599 (1986).
57. P. G. Bolhuis, D. Chandler, C. Dellago, P. L. Geissler, Transition path sampling: Throwing ropes over rough mountain passes, in the dark. *Annu. Rev. Phys. Chem.* **53**, 291–318 (2002).
58. D. Wang, R. Zhao, J. D. Weeks, P. Tiwary, Influence of long-range forces on the transition states and dynamics of NaCl ion-pair dissociation in water. *J. Phys. Chem. B* **126**, 545–551 (2022).
59. A. Rimola, M. Sodupe, P. Ugliengo, Amide and peptide bond formation: Interplay between strained ring defects and silanol groups at amorphous silica surfaces. *J. Phys. Chem. C* **120**, 24817–24826 (2016).
60. A. Rimola, M. Fabbiani, M. Sodupe, P. Ugliengo, G. Martra, How does silica catalyze the amide bond formation under dry conditions? Role of specific surface silanol pairs. *ACS Catal.* **8**, 4558–4568 (2018).
61. S. M. Piontek, A. Tuladhar, T. Marshall, E. Borguet, Monovalent and divalent cations at the α-Al_2O_3(0001)/water interface: How cation identity affects interfacial ordering and vibrational dynamics. *J. Phys. Chem. C* **123**, 18315–18324 (2019).
62. L. Zhang, C. Tian, G. A. Waychunas, Y. R. Shen, Structures and charging of α-alumina (0001)/water interfaces studied by sum-frequency vibrational spectroscopy. *J. Am. Chem. Soc.* **130**, 7686–7694 (2008).
63. M.-P. Gaigeot, M. Sprik, M. Sulpizi, Oxide/water interfaces: How the surface chemistry modifies interfacial water properties. *J. Phys. Condens. Matter* **24**, 124106 (2012).
64. X. Liu, J. Cheng, M. Sprik, X. Lu, R. Wang, Understanding surface acidity of gibbsite with first principles molecular dynamics simulations. *Geochim. Cosmochim. Acta* **120**, 487–495 (2013).
65. R. Wang, M. DelloStritto, M. L. Klein, E. Borguet, V. Carnevale, Topological properties of interfacial hydrogen bond networks. *Phys. Rev. B* **110**, 014105 (2024).
66. L. Lutterotti, P. Scardi, Simultaneous structure and size-strain refinement by the Rietveld method. *J. Appl. Cryst.* **23**, 246–252 (1990).
67. M. Parrinello, A. Rahman, Polymorphic transitions in single crystals: A new molecular dynamics method. *J. Appl. Phys.* **52**, 7182–7190 (1981).
68. S. Nosé, M. L. Klein, Constant pressure molecular dynamics for molecular systems. *Mol. Phys.* **50**, 1055–1076 (1983).
69. G. Bussi, D. Donadio, M. Parrinello, Canonical sampling through velocity rescaling. *J. Chem. Phys.* **126**, 014101 (2007).
70. B. Hess, P-LINCS: A parallel linear constraint solver for molecular simulation. *J. Chem. Theory Comput* **4**, 116–122 (2008).
71. U. Essmann, L. Perera, M. L. Berkowitz, T. Darden, H. Lee, L. G. Pedersen, A smooth particle mesh Ewald method. *J. Chem. Phys.* **103**, 8577–8593 (1995).
72. A. D. MacKerell, D. Bashford, M. Bellott, R. L. Dunbrack, J. D. Evanseck, M. J. Field, S. Fischer, J. Gao, H. Guo, S. Ha, D. Joseph-McCarthy, L. Kuchnir, K. Kuczera, F. T. K. Lau, C. Mattos, S. Michnick, T. Ngo, D. T. Nguyen, B. Prodhom, W. E. Reiher, B. Roux, M. Schlenkrich, J. C. Smith, R. Stote, J. Straub, M. Watanabe, J. Wiórkiewicz-Kuczera, D. Yin, M. Karplus, All-atom empirical potential for molecular modeling and dynamics studies of proteins. *J. Phys. Chem. B* **102**, 3586–3616 (1998).
73. A. D. Mackerell Jr., M. Feig, C. L. Brooks III, Extending the treatment of backbone energetics in protein force fields: Limitations of gas-phase quantum mechanics in reproducing protein conformational distributions in molecular dynamics simulations. *J. Comput. Chem.* **25**, 1400–1415 (2004).
74. R. T. Cygan, J.-J. Liang, A. G. Kalinichev, Molecular models of hydroxide, oxyhydroxide, and clay phases and the development of a general force field. *J. Phys. Chem. B* **108**, 1255–1266 (2004).
75. H. J. C. Berendsen, J. R. Grigera, T. P. Straatsma, The missing term in effective pair potentials. *J. Phys. Chem.* **91**, 6269–6271 (1987).
76. M. J. Abraham, T. Murtola, R. Schulz, S. Páll, J. C. Smith, B. Hess, E. Lindahl, GROMACS: High performance molecular simulations through multi-level parallelism from laptops to supercomputers. *SoftwareX* **1-2**, 19–25 (2015).
77. G. A. Tribello, M. Bonomi, D. Branduardi, C. Camilloni, G. Bussi, PLUMED 2: New feathers for an old bird. *Comput. Phys. Commun.* **185**, 604–613 (2014).
78. N. Michaud-Agrawal, E. J. Denning, T. B. Woolf, O. Beckstein, MDAnalysis: A toolkit for the analysis of molecular dynamics simulations. *J. Comput. Chem.* **32**, 2319–2327 (2011).
79. W. Humphrey, A. Dalke, K. Schulten, VMD: Visual molecular dynamics. *J. Mol. Graph.* **14**, 33–38 (1996).
80. J. D. Hunter, Matplotlib: A 2D graphics environment. *Comput. Sci. Eng.* **9**, 90–95 (2007).
81. G. Bussi, A. Laio, Using metadynamics to explore complex free-energy landscapes. *Nat. Rev. Phys* **2**, 200–212 (2020).
82. R. B. Best, X. Zhu, J. Shim, P. E. M. Lopes, J. Mittal, M. Feig, A. D. J. MacKerell, Optimization of the additive CHARMM all-atom protein force field targeting improved sampling of the backbone ϕ, ψ and side-chain X_1 and X_2 dihedral angles. *J. Chem. Theory Comput.* **8**, 3257–3273 (2012).
83. W. L. Jorgensen, D. S. Maxwell, J. Tirado-Rives, Development and testing of the OPLS all-atom force field on conformational energetics and properties of organic liquids. *J. Am. Chem. Soc.* **118**, 11225–11236 (1996).
84. G. Tzvetkov, G. Koller, Y. Zubavichus, O. Fuchs, M. B. Casu, C. Heske, E. Umbach, M. Grunze, M. G. Ramsey, F. P. Netzer, Bonding and structure of glycine on ordered Al_2O_3 film surfaces. *Langmuir* **20**, 10551–10559 (2004).
85. C. Arrouvel, B. Diawara, D. Costa, P. Marcus, DFT periodic study of the adsorption of glycine on the anhydrous and hydroxylated (0001) surfaces of α-alumina. *J. Phys. Chem. C* **111**, 18164–18173 (2007).
86. E. R. Beyerle, P. Tiwary, Thermodynamically optimized machine-learned reaction coordinates for hydrophobic ligand dissociation. *J. Phys. Chem. B* **128**, 755–767 (2024).
87. P. M. Piaggi, O. Valsson, M. Parrinello, Enhancing entropy and enthalpy fluctuations to drive crystallization in atomistic simulations. *Phys. Rev. Lett.* **119**, 015701 (2017).
88. T. E. Gartner, P. M. Piaggi, R. Car, A. Z. Panagiotopoulos, P. G. Debenedetti, Liquid-liquid transition in water from first principles. *Phys. Rev. Lett.* **129**, 255702 (2022).

Acknowledgments: We thank M. DelloStritto for fruitful discussions. **Funding:** This work was supported as part of the Center for Complex Materials from First Principles (CCM), an Energy Frontier Research Center funded by the U.S. Department of Energy, Office of Science, Basic Energy Sciences under Award #DE-SC0012575 (E.B.). This work was funded by the National Institutes of Health (R01GM093290, R01GM131048, and S10OD020095 to V.C.) and the National Science Foundation (grant IOS-1934848 to V.C. and grant CHE 2102557 to E.B.). This research includes calculations carried out on HPC resources supported in part by the National Science Foundation through major research instrumentation grant numbers 1625061 and 2216289 and by the US Army Research Laboratory under contract numbers W911NF2120007 (M.L.K.) and W911NF-16-2-0189. R.C.R. acknowledges support from the National Aeronautics and Space Administration Exobiology Program under grant number 80NSSC20K0609. **Author contributions:** Conceptualization: R.W., R.C.R., M.L.K., E.B., and V.C. Methodology: R.W., R.C.R., M.L.K., E.B., and V.C. Investigation: R.W. Visualization: R.W. Supervision: R.C.R., M.L.K., E.B., and V.C. Writing—original draft: R.W. Writing—review and editing: R.W., R.C.R., M.L.K., E.B., and V.C. **Competing interests:** The authors declare that they have no competing interests. **Data and materials availability:** Files to set up simulations are available at https://github.com/ruiyuwangwork/GLY_Alumina and https://doi.org/10.5281/zenodo.14607062. All data needed to evaluate the conclusions in the paper are present in the paper and/or the Supplementary Materials.

Submitted 12 October 2024
Accepted 6 March 2025
Published 11 April 2025
10.1126/sciadv.adt4151